Modes of the southern extension of the East Madagascar Current

Gerold Siedler[1,2], Mathieu Rouault[2], Arne Biastoch[1], Bjorn Backeberg[2,3], Chris J.C. Reason[2], and Johann R. E. Lutjeharms[2]

[1]Leibniz-Institute for Marine Sciences (IFM-GEOMAR),

Kiel University, 24105 Kiel, Germany

[2]Department of Oceanography,

University of Cape Town, Private Bag X3,

Rondebosch, 7701, South Africa

[3]Mohn-Sverdrup Center for Global Ocean Studies and Operational Oceanography

Thormøhlensgt. 47

5006 Bergen, Norway

Corresponding author:

Dr. Gerold Siedler, IFM-GEOMAR, Düsternbrooker Weg 20, 24105 Kiel, Germany.

E-mail: gsiedler@ifm-geomar.de

Abstract

Data sets from satellite observations and a nested high-resolution model are used to study a source region of the Agulhas Current. Altimeter-derived geostrophic surface currents are averaged over varying periods, providing evidence of the persistence of flow patterns in the extension of the southern branch of the East Madagascar Current (SEMC). South of Madagascar, the SEMC separates into one branch towards the Agulhas Current and into a second branch retroflecting and connecting to the Subtropical Indian Ocean Countercurrent (SICC). Good agreement is found between long-term mean patterns of observational and model dynamic heights. Two basic modes are identified in the SEMC extension, with anticyclonic motion favoring retroflection in the northern Mozambique Basin when the extension is in a south-westward direction and cyclonic motion occurring in the case of the SEMC flowing westward along the southern Madagascar slope. A cross-correlation sequence between model SEMC transports and the modal changes in the extension region displays a correlation at about one-month lag which agrees with eddy propagation time from the SEMC to the outflow region. Mean model SEMC transports are determined using floats released at 21°S, and the contribution of the SEMC to the SICC is obtained using floats injected at 55°E with the model running backwards. Almost half of the SEMC volume transport contributes to the Agulhas system, and about 40% of SICC water originates from the SEMC.

1.Introduction

The western boundary current system of the South Indian Ocean (Fig. 1) is strongly influenced by the island of Madagascar (Penven et al., 2006) and consists of the East Madagascar Current at subtropical latitudes and the stronger Agulhas Current (AC) further south (Lutjeharms, 2006). No persistent boundary current exists in the Mozambique Channel west of Madagascar although water masses are transferred along the Mozambique coast to the south by large and deep anti-cyclonic eddies (de Ruijter et al., 2002; Schouten et al., 2002a). The southern branch of the East Madagascar Current (SEMC) has been considered a source for the AC (Stramma and Lutjeharms, 1997; Biastoch and Krauss, 1999; Biastoch et al., 1999; de Ruijter et al., 2004; Quartly et al., 2006). The region from the south of Madagascar to the African coast links the SEMC and the Mozambique Channel transports with the AC and therefore represents a source region for the AC system. Moreover, perturbations in the form of eddies that originate from these source regions have been implicated in generating disturbances in the Agulhas Current proper and thus in inter-ocean leakage south of Africa (de Ruijter et al., 2004; van Leeuwen et al., 2000).

The SEMC is fed by the southern core of the South Equatorial Current which is topographically guided towards the west through a gap in the Mascarene Plateau/Wilshaw Ridge (see Fig. 1) north of Mauritius (New et al., 2007). Upon arrival at the eastern slope of Madagascar at about 18 - 19°S it branches to the north and south. The southward flow of the SEMC reaches as deep as 1100 m at 22°S, with volume transports estimated at about 21 Sv (1 Sv = 1 Sverdrup = 10^6 m^3 s^{-1}) on the basis of hydrographic and moored current meter observations (Swallow, et al., 1988; Schott et al., 1988). Hydrographic observations show the

SEMC clinging to the slope connecting the Madagascar shelf and the deep Madagascar Basin further south (Lutjeharms et al., 1981; Donohue and Toole, 2003) while approaching the southern tip of Madagascar. Overall, however, the track and strength of the SEMC are not well documented due to the scarcity of *in situ* data.

The region east of the SEMC near 25°S is characterized by strong disturbances in the flow field, propagating from east to west across the South Indian Ocean until they arrive at the eastern side of Madagascar. Birol and Morrow (2001, 2003) and Schouten et al. (2002b) attributed them to Rossby waves while Quartly et al. (2006) considered them more likely to be a train of propagating eddies. Chelton et al. (2007) found that much of the mesoscale variability outside the tropics consists of nonlinear eddies propagating westward at the phase speed of baroclinic Rossby waves, thus supporting the latter interpretation.

The SEMC extension to the south and southwest of Madagascar is dominated by a rich eddy field. Eddies in this region have been extensively studied on the basis of remote-sensing observations (Gründlingh et al., 1991; Gründlingh, 1995; de Ruijter et al., 2004; Quartly et al., 2006), documenting cyclonic (clockwise) and anticyclonic (counterclockwise) eddies propagating from Madagascar to the west and southwest towards the AC region. Lutjeharms et al. (1981) and Lutjeharms (1988) have suggested a retroflection of the SEMC south of Madagascar to the east and an intermittent flow to the west feeding the AC. Quartly et al. (2006) by contrast concluded that no persistent retroflection exists because it would require long-term eastward flow at 25°-30°S. The subsequent studies of Siedler et al. (2006) and Palastanga et al. (2007) have, however, documented the existence of an eastward South Indian Ocean Countercurrent (SICC) near 25°S within transient migratory cyclones and anti-

cyclones. Evidence of a branching of the mean current and the existence of the SEMC retroflection was established by Siedler et al. (2006) using multi-year means of absolute geostrophic current fields with high resolution from altimeter data (Rio and Hernandez, 2004).

It is the goal of the present study to provide an improved understanding of the role of the SEMC extension in the AC source region. Using altimeter and model data, we will provide evidence for the persistency of the branching and retroflection of the SEMC extension, we will identify dominating modes in the eddy currents and search for key processes controlling such modes, and we will determine model transports in order to quantify the contributions of the SEMC to the AC and the SICC.

2. The observations

The primary observational data set for the present study originates from a combination of altimetric data, *in situ* measurements and a geoid model. Rio and Hernandez (2004) subtracted altimetric sea surface heights (1993 – 1999) from a geoid model. Filtering was applied to retain only the spatial scales for which the geoid is accurate enough, resulting in an effective resolution of about 660 km. This mean dynamic topography estimate was then improved by locally subtracting the altimetric variability from the absolute oceanographic signal obtained from *in situ* measurements. Absolute geostrophic velocities can then be obtained from the dynamic topographies. The method allows a continuous integration of new data and an extension of the time series.

To derive an improved dynamic topography, Rio et al. (2005) used a better geoid model resulting from GRACE satellite measurements and an updated *in situ* data set with drifter and hydrographic observations that were not included earlier in the estimation process. Their spatial resolution of the final data set is around 50 – 100 km, and their estimates of root mean square differences between altimetric heights and in situ dynamic heights for the Indian Ocean equatorward of 40° lead to geostrophic velocity errors between about 13cm/s (eastward component) and 14 cm/s (northward component). Rio and Hernandez (2004) showed values near 10 cm/s in the central subtropical South Indian Ocean, but larger errors in strong western boundary currents such as the Agulhas Current. The errors near Madagascar appeared to be less than 15 cm/s. The AVISO product CMDT RIO05 in version DT-MADT "Ref" is used in the present study, with high-resolution maps of absolute geostrophic velocities derived from maps of dynamic topography, combining data from Topex/Poseidon and Jason-1 + ERS, Envisat.

The second observational data set comprises ocean color data from SeaWiFS which measures light intensity in several radiation bands. The measurements allow quantification of light absorption and subsequent estimation of chlorophyll_a concentrations. The images and data used in this study were acquired using the GES-DISC Interactive Online Visualization Analysis Infrastructure (Giovanni) as part of the NASA's Goddard Earth Sciences (GES) Data and Information Services Center (DISC). We used subsets of the “Giovanni Ocean Color Time-Series Online Visualization and Analysis(OBPG)” SeaWiFS Monthly Global 9-km Products, data version 5, reprocessing 5.2, July 2007. These data have been shown to be closely related to surface water mass patterns in the region (e.g. Quartly et al., 2006).

3. The model

Model data are obtained from a high-resolution (1/10°) model of the greater Agulhas region (20°W-70°E; 47°S-7°S) nested in a global coarse-resolution (1/2°) ocean sea-ice model (Biastoch et al. 2008a) based on the NEMO-Code (Madec, 2007). The model features state-of-the-art physics, such as advanced advection schemes and partially filled bottom cells (46 levels), both crucial elements for the reasonable simulation of the large-scale circulation (Barnier et al., 2006). The two grids are connected by a nesting approach (Debreu et al., 2005), allowing the high-resolution nest to receive its open boundary values from the coarse-resolution base model and, since this approach is two-way, to update the base model with data from the nest. This approach optimally embeds the Agulhas system into the large-scale circulation. The model system is forced by a consistent data set (Large and Yeager, 2004) of 6-hourly to daily, inter-annually varying wind and thermohaline forcing fields over the period 1958-2004. It has been demonstrated that the base model (ORCA05) simulates the large-scale circulation reasonably well (e.g. Biastoch et al., 2008a), while the high-resolution nest captures the transport and currents of all components of the greater Agulhas system with substantial success (Biastoch et al., 2008b). These authors have demonstrated that the mesoscale variability around southern Africa, including the perturbations in the Mozambique Channel and east of Madagascar, is represented realistically in comparison with satellite altimetry. They follow up earlier studies (Schouten et al., 2002a, Penven et al., 2006) documenting that upstream perturbations in the source regions of the Agulhas system

have a connection to the shedding of Agulhas rings and univocally demonstrate the importance of mesoscale variability for the inter-ocean exchange south of Africa.

4. The persistency of the SEMC branching and retroflection

Averaging the geostrophic current fields over many years will finally lead to the mean field provided by the RIO05 mean dynamic topography. We want to show that the SEMC/retroflection/SICC pattern is a persistent feature on shorter time scales of only a few years. Fig. 2 provides an example of an individual geostrophic current map that shows major anticyclonic and cyclonic motion southwest of Madagascar and the energetic eddy field east of the island. One notes the consistent eastward flow in the wave-like pattern at 25° S. With the intense eddies/planetary waves dominating the upper-ocean flow in the region, averaging over periods longer than those characteristic of eddies and waves is needed to extract mean currents. We used various averaging periods to identify the SEMC branching and retroflection. Typical examples are presented in Fig. 3. The average over the second half of 2002 (Fig. 3a) shows the outflow from the SEMC to the south-west and further on towards the AC, with a weak retroflection and a patchy current pattern further south and also east of southern Madagascar. The averaging over the full year 2002 (Fig. 3b) still produces a patchy current pattern, but with the retroflection of the SEMC expressed much more strongly. Averaging over two years (Fig. 3c) further strengthens the retroflection branch. The transition to the flow regime east of Madagascar stands out more clearly in the three-year mean (Fig. 3d), as does the SICC band in the range between 55° and 60° E. Further east (only

partly shown in Fig.3) much shorter averaging periods are usually sufficient to show the SICC band.

Maximenko et al. (2005) have questioned whether zonal jets in the world ocean observed by altimeters are real or instead are propagating eddies smoothed in time. Averaged individual eddies moving westward along a specific latitude would produce zonal jets both to the west and the east depending on the ratio between azimuthal and propagating speeds. Lengthening the averaging period will reduce the corresponding meridional currents. Also, a mix of cyclonic and anticyclonic eddies will weaken the jets when an extended averaging time is used.

With respect to the SEMC retroflection, a reduction of the meridional transport with increasing averaging period is not observed, and in fact, just the opposite is the case. The flow to the south in the retroflection region emerges more clearly with a longer averaging period. Maximenko et al. (2005) have also discussed the fact that averaging in time over a westward propagating eddy would produce a zonally elongated structure with its length defined by the displacement of the eddy during the averaging period. They found that the characteristic near-zonal lengths of jets in the North Pacific subtropical region exceed the estimated displacements of eddies by a factor of 3 -5 on weekly maps and 2 – 2.5 for 18-week averages. In our case, when inspecting 3-month averages of the altimeter-derived geostrophic surface currents near 25° S and east of 60° E (only partly shown here), elongated structures are often found with an extension between 60°E and 80°E , corresponding to approximately 2000 km. When comparing with an eddy displacement of about 500 km resulting from a phase speed around 6 km/day (Birol and Morrow, 2001), the factor is near

4. Also, the eddy field at these latitudes comprises both cyclonic and anticyclonic eddies (Chelton et al., 2007), and no additional transport bands to the west are observed near 25°S. These properties provide evidence that the observed mean flow to the east is real and not an artifact of eddy-smoothing. We also note that Huang et al. (2007) found quantitative support for basin-wide zonality in their study of anisotropy in Pacific mid-ocean currents.

Interannual and longer-term changes cause some variability in the above altimeter-derived patterns if averaging is performed over different years. But the general conclusion is: although at any given time the circulation is transient with migratory cyclones and anti-cyclones, the mean flow towards the AC and the retroflection of the SEMC is always evident when averaging over two years or longer. We note that the average retroflection loop is found near 42°E and so further west than was assumed by Lutjeharms (1988). The flow turns around in the northern Mozambique Basin, at some distance to the west from the shallower Madagascar Plateau (< 2 000 m) that lies directly to the south of Madagascar (see Fig. 1). The basic mean pattern is consistent with the mean dynamic topography and corresponding geostrophic circulation presented in Fig. 15 of Rio and Hernandez (2004) on a 1°x1° grid. The updated Aviso data (Rio et al., 2005) are provided on a 1/3°x1/3° grid, and the mean current bands with the use of the more recent data set appear narrower by a factor of two to three in our results.

5. Modes of the SEMC extension

Fig. 4 derived from the model clearly represents the main features of the large scale circulation in the South West Indian Ocean; namely the westward South Equatorial Current north of Madagascar, which then partially leads into a southward flow through the Mozambique Channel between Madagascar and the African mainland, the Agulhas Current along the South African coastline and the retroflection into the eastward Agulhas Return Current between 35 and 45° S.

For an initial comparison of the results from our observational and model data sets, we present sea surface height (SSH) maps averaged over the three years 2001-2003 in Fig. 5. Due to mapping techniques in the basic maps the contoured SSH in Fig. 5a reaches into the near-coastal areas without data coverage. The thick lines indicate general agreement between the observations and model in the SEC inflow towards Madagascar near 18-19°S, the outflow from the SEMC south of the island, the retroflection near 41–42°E and the continuation into the SICC near 25°S.

In the model output, the core of the SEMC is clearly recognized near the slope of eastern Madagascar, being fed by the SEC and providing the jet-like transport to the west-southwest towards the northern Mozambique Basin. The retroflection is there, but not as distinct as it is in the observational data. The current returning from the retroflection to the east, then to the north and finally feeding the SICC is quite similar to what was seen in the observational results above.

Because the altimeter dataset which we use does not have values close to the coast of Madagascar we rely on model results for an inspection of the SEMC and its transition into

the southern extension. In Fig. 4, one recognizes the southward SEMC along the eastern Madagascar coastline and its outflow in a southwestward to westward direction south of Madagscar. We selected a sample with a strong reduction of the SEMC at the eastern Madagascar slope between 22 and 24° S which will be discussed later. Cyclonic motion is seen in the northern Mozambique Basin north of the outflow core while anticyclonic motion occurs south of the core. They represent examples of a pattern with two modes which is typical for the SEMC outflow region.

Two further examples are given to illustrate the modal structure. Satellite ocean color images have been used earlier to describe flow patterns in the region (DiMarco et al., 2000; Lutjeharms and Machu, 2000; Quartly et al., 2006). High nutrient content and chlorophyll concentrations exist around southern Madagascar due to upwelling. The SEMC carries the chlorophyll away from the coastal region over some distance until the signal disappears due to mixing and biological mortality. From the Giovanni Ocean Color Time-Series Online Visualization and Analysis, OBPG SeaWiFS Monthly Global 9-km Products, we present two cases in Fig. 6 to demonstrate the modal structure. The chlorophyll_a pattern for the monthly mean of July 2005 on the left side of Fig. 6a shows an example of a zonally-oriented plume south of Madagascar with a source region further east. The altimeter-derived geostrophic surface currents on the right side have corresponding patterns. One has to keep in mind, however, that there can be events where interaction with Mozambique Channel eddies plays a role. Quartly and Srokosz (2004) have previously shown that cyclonic motion to the south-west of Madagascar can sometimes also be due to eddies propagating southward on the eastern side of the Mozambique Channel. The monthly mean for

November 2005 in Fig. 6b shows only the south-westward plume. The chlorophyll plume does not reach far enough here to show the retroflection itself.

Although these patterns change between different samples, there exists a pattern of two modes on the average which is found both in the observational and model data sets when determining the fields of negative (cyclonic) and positive (anticyclonic) relative vorticity. For each time-step the areas with positive and negative vorticity were located and stored. By calculating the eddy kinetic energy (EKE = ½ ($u'^2 + v'^2$) with eastward velocity u = umean + u' and northward velocity v = vmean + u') in those areas where cyclonic or anticyclonic motion occurs, one arrives at the respective contributions of cyclonic or anticyclonic EKE to the total EKE.

Averages from 1 Jan 1996 to 31 Dec 2005 of the resulting fields of cyclonic and anticyclonic EKE are presented in Fig. 7. The upper sub-figures represent the EKE distributions for the model and the lower sub-figures for the altimeter data. One notes maxima of cyclonic and anticyclonic EKE existing in the SEMC outflow region at somewhat different latitudes, with the cyclonic EKE maximum further north than the anticyclonic one. The cyclonic and the anticyclonic EKE fractions of the total EKE are given in Fig. 8. The inserted boxes approximately mark the maxima of cyclonic and anticyclonic EKE fractions in the SEMC outflow region. These boxes are also given in Fig.7 for reference. The patterns from the altimeter and model data are similar, but not exactly the same. We therefore selected different box sizes and positions for the observational and model data.

The EKE per area values are summarized in Table 1. Although one finds a clear bi-modal maximum/minimum pattern in each fraction sub-figure of Fig.8, the contributions to the total EKE are only around 0.5-0.6 in the maxima for the observations while they are near 0.65-0.7 for the model.

High-resolution SSH anomalies from altimeters have been used to determine the differences in global patterns of tracks of eddies with opposing sign of vorticity (Chelton et al., 2007). A subset of eddy tracks for the Agulhas source region was provided by D. B. Chelton and is shown in Fig. 9. The maximum of cyclonic motion is seen west of the southern tip of Madagascar while a range of anticyclonic motion is found at the southern end of this maximum range and from there to the east and northeast, along the flow track from the retroflection to the SICC (see Fig. 3d). These frequency distributions correspond to the two preferred flow modes in the SEMC extension which were identified above. Fig. 10 provides a schematic of the two modes. What might be the cause of the variations in the SEMC outflow properties which result in these two modes of flow behavior? We suggest that interaction between the eddy/wave train arriving at the south-eastern slope of Madagascar from the east and the SEMC has a major effect on this bi-modal flow variability. The model sample in Fig.4 showed an increased eddy field around 25° S east of Madagascar. The region corresponds to the area where a maximum of mean kinetic eddy which was already found in the model study of Biastoch and Krauss (1999).

The model sample in Fig.4 showed a weak SEMC around 22-24° S, seemingly related to the neighboring eddy field. The early mooring observations by Schott et al. (1988) showed similar cases of strong reduction or even reversal of the SEMC at 22°S on time scales of a

month. Could a weakening or strengthening of the SEMC due to interaction with the eddy field influence the vorticity pattern in the SEMC outflow south of Madagascar?

The maximum of cyclonic motion in the outflow region is to the west of the southern tip of Madagascar. In a westward flow, planetary vorticity will not change. When analyzing tracks of eddies in altimeter data sets for 1995 – 2000, de Ruijter et al. (2004) suggested that friction in the westward flow at the inshore edge of the SEMC will produce cyclonic relative vorticity, in agreement with the above cyclonic motion. However, when the SEMC overshoots the slope towards the west-southwest, moving into deep water beyond the Madagascar Plateau to the Mozambique Basin, these frictional effects will not be present. For the southward component of the SEMC, the planetary vorticity changes and in order to conserve absolute vorticity, anti-cyclonic motion results. This conclusion is confirmed by the eddy tracks in Fig. 9 of de Ruijter et al. (2004). Their tracks of cyclonic eddies were consistently found closer to the shelf south of Madagascar than those of the anticyclones. There also appear to exist similarities with conditions in the Agulhas Current retroflection where Dijkstra and de Ruijter (2001) concluded that inertial overshoot and subsequent compensation of increasing positive relative vorticity by negative relative vorticity lead to retroflection, and similarities with the generation of cyclonic lee eddies from the Agulhas Current at the continental shelf (Penven et al., 2001).

If the EKE variations in the SEMC outflow were related to a weakening or strengthening of the SEMC, one would expect a lagged correlation between SEMC transports and EKE levels in the regions of maximum cyclonic and anticyclonic motion. In Fig. 11, we present model time series of the SEMC transport at 21° S (0-1300 m, Madagascar coast to 51° E) and the absolute

values of vorticity in the boxes shown in Fig. 7. The 5-day series (Fig. 7a) show time scales from weeks to years while only longer time scales appear in Fig. 7b where a 2-month moving average was applied. In the high-resolution series above, we frequently identify short-term (about 1-2 months) events in the vorticity time series with similar in-phase variations in both vorticity series, but there are also events where the changes are out-of-phase. The in-phase variations imply a simultaneous strengthening of the cyclonic and anticyclonic motion in the boxes, with a possible dipole appearance. By contrast, the out-of-phase changes suggest a strengthening of one mode only. Although individual events often appear to be correlated, the overall correlation may be marginal.

The corresponding Figs.7c and 7d are given for the model, with the addition of the 21° S transports. The correspondence between events in the transport and vorticity time series on the short time scales are less obvious although there are several events where similar behavior is recognized, in particular in the anticyclonic vorticity and the transport time series. The smoothed time series below indicate approximately bi-annual transport changes while changes with scales of several months to half a year seem to dominate the vorticity changes.

We determined the cross-correlation sequence between the transport and the two vorticity time series to search for correspondences and for dominating time scales (Fig. 12). For both the cyclonic and the anti-cyclonic case we find significant peaks at about one month which indicate the changes in the outflow lagging behind the changes in the SEMC transport. There is also a significant peak for cyclonic motion at 3-4 months.

The one-month scale corresponds to the approximate travel time of eddies from the 21° S region to the outflow boxes as earlier shown in Hovmoller diagrams e.g. by Schouten et al. (2002b). The 3-4 months scale may be related to the sequence of events in the zonal wave/eddy band at 25° S (Birol and Morrow, 2001, 2003; Schouten et al., 2002b).

6. Volume transports feeding the AC and the SICC

In order to quantify the amount of waters leaving the SEMC and arriving at the SICC, an offline Lagrangian diagnostic (ARIANE; Blanke et al., 1999) was used. O(10^5) floats were released over the southward flowing SEMC at 21°S (Fig. 13), each representing a small part (maximum 0.01 Sv) of the volume transport, and advected using the 5-daily averaged velocity output of the model. To capture the full variability of the transport, floats were seeded continuously over a period of 3 years (1995-1997). After the seeding ended, the volume transport represented by the floats was integrated for another 7 years (1998-2004), so that at the end virtually all floats had crossed one of the control sections which form a box around the region. These floats with their respective transports were counted when leaving the box spanned by the individual control sections. The sum for each section provides the time-mean transport. However, since the advection times towards the receiving stations span a certain time spectrum, the resulting transport cannot be related to certain release dates, and no standard deviation can be given.

Almost half (48%, Table 2) of the total model transport of 16 Sv (± 4.5 Sv standard deviation) flows towards the Agulhas Current, another 41% flows eastward back into the central Indian Ocean (with a minor portion flowing south). About one third of the water remaining in the central Indian Ocean leaves the control volume to the north, with some already in the vicinity of the SEMC, thus indicating the eddying structure of this western boundary current. Slightly more than 10% of the total SEMC transport leaves the region via the SICC.

A similar strategy was used for identifying the sources of the SICC (Fig. 14), but in this case the float displacements were integrated backwards (seeded 2004-2002, and further integrated 2001-1995). Here, a significant portion (40%, Table 3) of the water enters the control volume via the northern boundary, either with the SEMC or offshore of the western boundary current. Almost half of the total SICC transport enters via the eastern boundary, again underlining the strong eddying structure in the central Indian Ocean. Less than 10% is fed from southern sources, and virtually no water enters the SICC from the Agulhas regime.

7. Conclusions

Averaged altimeter-derived and high-resolution model data sets are consistent in describing the mean flow from the SEC through the SEMC to the outflow region, with branches leading into the Agulhas Current and through a retroflection and a close approach to the SEMC at the south-eastern tip of Madagascar towards the SICC. An averaging of altimeter current maps over about two years is sufficient to determine a persistent mean flow pattern.

Two modes in vorticity are found in the extension region of the SEMC. The fraction of anticyclonic motion has a maximum in the northern Mozambique Basin where the retroflection was identified, while the fraction of cyclonic motion has a maximum further north. The area of maximum anticyclonic motion stretches from the retroflection region to the east and northeast, essentially following the track of the retroflected water towards the SICC.

A correspondence of events on time scales of 1-2 months is frequently observed. However, they are sometimes in-phase and sometimes out-of-phase. Significant cross-correlation between model time series of transport at 21° S and vorticity magnitudes in the cyclonic and anticyclonic maximum regions is found at time scales of about one month and at 3-4 months, with the outflow region changes lagging behind the SEMC transport changes. The one-month time scale corresponds to the approximate travel time of eddies from 21° S to the maximum regions while 3-4 months correspond to typical event sequences in the wave/eddy train at 25° S. The release of floats at a section across the SEMC in the model permits one to follow the SEMC outflow and to provide transport estimates. Almost 50 % of the total SEMC transport into the control volume heads towards the Agulhas Current while about 40 % flows back into the central Indian Ocean. Only about 10 % moves to the south. When releasing floats at a section across the SICC and running the model backwards one can check whether the SEMC region provides a source for the SICC. About 40 % of the float transport originates from the northern boundary of the control volume which includes the SEMC and the region to the east up to the Wilshaw Ridge. The SEMC is thus an important contributor to the greater Agulhas system, and the SICC receives a large amount of source water from the SEMC region.

Acknowledgements

The altimeter products used in this study were produced by Ssalto/Duacs and distributed by Aviso with support from Cnes. Rio05 was produced by CLS Space Oceanography Division. (http://www.aviso.oceanobs.com/en/data/products/sea-surface-height-products/global/madt/index.html). Ocean color data were produced by the SeaWiFS Project at Goddard Space Flight Center. The images and data used in this study were acquired using the GES-DISC Interactive Online Visualization and Analysis Infrastructure (Giovanni) as part of the NASA's Goddard Earth Sciences (GES) Data and Information Services Center (DISC) (http://reason.gsfc.nasa.gov/OPS/Giovanni/ocean.seawifs.shtml). Use of these data is in accord with the SeaWiFS Research Data Use Terms and Conditions Agreement. The integration of the model experiments has been performed at the Höchstleistungsrechenzentrum Stuttgart (HLRS), Germany. The bathymetry in Figures 1 and 10 was extracted from the GEBCO Digital Atlas published by the British Oceanographic Data Centre on behalf of the IOC and IHO, 2003. The study was supported by the National Research Foundation, the Water Research Commission, and the University of Cape Town in South Africa, and the Deutsche Forschungsgemeinschaft (DFG, project number BO 907/2-2) and the Leibniz Institute for Marine Sciences (IFM-GEOMAR) at Kiel University in Germany. The provision of Fig. 9 with recent results on eddy patterns by D.Chelton was much appreciated. G. S. expresses his gratitude for the Alexander von Humboldt Award that made this study possible.

Reference list

Barnier, B., G. Madec, T. Penduff, J.-M. Molines, A.-M. Treguier, J. Le Sommer, A. Beckmann, A. Biastoch, C. Böning, J. Dengg, S. Gulev, C. Derval, E. Durand, E. Remy, C. Talandier, S. Thetten, M. Maltrud, J. McLean, and B. de Cuevas, (2006), Impact of partial steps and momentum advections schemes in a global ocean circulation model at eddy permitting resolution. *Ocean Dynamics, 56*(5-6), 543-567, doi: 10.1007/s10236-006-0082-1.

Biastoch, A., C. J. C. Reason, J. R. E. Lutjeharms, , and O. Boebel (1999), The Importance of flow in the Mozambique Channel to seasonality in the greater Agulhas Current system, *Geophysical Research Letters, 26*, 3321-3324.

Biastoch, A., and W. Krauss (1999), The role of mesoscale eddies in the source regions of the Agulhas Current, *Journal of Physical Oceanography*, *29*, 2303–2317.

Biastoch, A., C. Böning, J. Getzlaff, J.-M. Molines, and G. Madec (2008a), Causes of interannual - decadal variability in the meridional overturning circulation of the mid-latitude North Atlantic Ocean, submitted to *Journal of Climate*

Biastoch, A., J. R. E. Lutjeharms, C. W. Böning, and M. Scheinert (2008b), Meso-scale perturbations control inter-ocean exchange south of Africa, under review at *Nature Geoscience*.

Birol, F., and R. Morrow (2001), Source of the baroclinic waves in the southeast Indian Ocean, *Journal of Geophysical Research, 106*, 145 - 160.

Birol, F., and R. Morrow (2003), Separation of quasi-semiannual Rossby waves from the eastern boundary of the Indian Ocean, *Journal of Marine Research, 61*, 707-723.

Blanke, B., M. Arhan, S. Speich, and G. Madec, G. (1999), Warm water paths in the equatorial Atlantic as diagnosed with a general circulation model. *J. Phys. Oceanogr*., *29*, 2753-2768.

Chelton, D. B., M. G. Schlax, R. M. Samelson, and R. A. de Szoeke (2007), Global observations of large oceanic eddies, *Geophysical Research Letters*, *34*, L15606, doi:10.1029/2007GL030812.

de Ruijter, P. M., H. M. van Aken, E. J. Beier, J. R. E. Lutjeharms, R. P. Matano, and M. W. Schouten (2004), Eddies and dipoles around South Madagascar: formation, pathways and large-scale impact, *Deep-Sea Research I*, *51*, 383–400.

de Ruijter, W. P. M., H. Ridderinkhof, J. R. E. Lutjeharms, M. W. Schouten, and C. Veth (2002), Observations of the flow in the Mozambique Channel, *Geophysical Research Letters*, 29 (10), 1502, 10.1029/2001GL013714.

Debreu, L., E. Blayo, and B. Barnier (2005), A general adaptive multi-resolution approach to ocean modelling: experiments in a primitive equation model of the north Atlantic, *Lecture*

Notes in Computational Science Engineering, adaptive mesh refinement - theory applications, 41, 303-313, doi:10.1007/3-540-27039-6_21.

Dijkstra, H. A., and W. P. M. de Ruijter (2001), On the Physics of the Agulhas Current: Steady Retroflection Regimes, Journal of Physical Oceanography 31, 2971-2985.

DiMarco, S. F., P. Chapman, and W. D. Nowlin, Jr. (2000), Satellite observations of upwelling on the continental shelf south of Madagascar, *Geophysical Research Letters*, *27*, 3965 – 3968.

Donohue, K. A., and J. M. Toole (2003), A near-synoptic survey of the Southwest Indian Ocean, *Deep-Sea Research II*, *50*, 1893– 1931.

Gründlingh, M. L. (1995), Tracking eddies in the southeast Atlantic and southwest Indian oceans with TOPEX/Poseidon, *Journal of Geophysical Research, 100*, 24977– 24986.

Gründlingh, M. L., R. A. Carter, and R. C. Stanton (1991), Circulation and water properties of the Southwest Indian Ocean, spring 1987, *Progress in Oceanography,* 28, 305-342.

Huang, H.-P., A. Kaplan, E. N. Curchitser, and N. A. Maximenko (2007), The degree of anisotropy for mid-ocean currents from satellite, observations and an eddy-permitting model simulation, *Journal of Geophysical Research, 112*, C09005, doi:10.1029/2007JC004105.

Large, W.G., and S. G. Yeager (2004), Diurnal to decadal global forcing for ocean and sea-ice models: the data sets and flux climatologies. *Technical Report NCAR/TN-460+STR*, NCAR, 105 pp.

Lutjeharms, J. R. E. (1988), Remote sensing corroboration of retroflection of the East Madagascar Current, *Deep-Sea Research, 35*, 2045-2050.

Lutjeharms, J. R. E. (2006), The Agulhas Current, Springer, Berlin, 329 pp.

Lutjeharms, J. R. E., and E. Machu (2000), An upwelling cell inshore of the East Madagascar Current, *Deep-Sea Research I*, *47*, 2405 – 2411.

Lutjeharms, J. R. E., N. D. Bang, and C. P. Duncan (1981), Characteristics of the current east and south of Madagascar, *Deep-Sea Research A*, *28*, 879 – 901

Madec, G. (2007), NEMO ocean engine. Note du Pole de mod´elisation, Institut Pierre-Simon Laplace (IPSL), France.

Maximenko, N. A., B. Bang, and H. Sasaki (2005), Observational evidence of alternating zonal jets in the world ocean. *Geophysical Research Letters*, Vol. 32, L12607, doi:10.1029/2005GL022728,

New A. L., S.G. Alderson, D. A. Smeed, and K. L. Stansfield (2007), On the circulation of water masses across the Mascarene Plateau in the South Indian Ocean, *Deep-Sea Research I, 54*, 42–74

Palastanga, V., P. J. van Leeuwen, M. W. Schouten, and W. P. M de Ruijter (2007), Flow structure and variability in the subtropical Indian Ocean: instability of the South Indian Ocean Countercurrent, *Journal of Geophysical Research, 112*, C01001, doi:10.1029/2005JC003395

Penven, P., J. R. E. Lutjeharms, P. Marchesiello, C. Roy, and S. J. Weeks (2001), Generation of cyclonic eddies by the Agulhas Current in the lee of the Agulhas Bank, Geophysical Research Letters, 28, 6,1055-1058.

Penven, P., J. R. E. Lutjeharms, and P. Florenchie (2006), Madagascar: A pacemaker for the Agulhas Current system?, Geophysical Research Letters, VOL. 33, L17609, doi:10.1029/2006GL026854

Quartly, G. D., and M. A. Srokosz (2004), Eddies in the southern Mozambique Channel, *Deep-Sea Research I*, *51*, 69 – 83.

Quartly, G. D., J. J. H. Buck, M. A. Srokosz, and A. C. Coward (2006), Eddies around Madagascar — The retroflection re-considered, *Journal of Marine Systems*, doi:10.1016/j.jmarsys.2006.06.001.

Rio, M. H., P. Schaeffer, F. Hernandez, and J.-M. Lemoine (2005), The estimation of the ocean Mean Dynamic Topography through the combination of altimetric data, in-situ measurements and GRACE geoid: From global to regional studies, *Proceedings of the GOCINA international workshop*, Luxembourg, 6 pp.

Rio, M.-H., and F. Hernandez (2004), A mean dynamic topography computed over the world ocean from altimetry, in situ measurements, and a geoid model, *Journal of Geophysical Research, 109*, C12032, doi:10.1029/2003JC002226.

Schott, F., M. Fieux, J. Kindle, J. Swallow, and R. Zantopp (1988), The boundary currents east and north of Madagascar 2. Direct measurements and model comparison, *Journal of Geophysical Research, 93*, 4963-4974.

Schouten M. W., W. P. M. de Ruijter, and P. J. van Leeuwen (2002a), Upstream control of Agulhas Ring shedding, *J. Geophys., Res., 107* (C8), 3109, doi:10.1029/2001JC000804.

Schouten, M. W., W. P. M. de Ruijter, P. J. van Leeuwen, and H. A. Dijkstra (2002b), An oceanic teleconnection between the equatorial and southern Indian Ocean. Geophysical Research Letters, VOL. 29, NO. 16, 1812, 10.1029/2001GL014542.

Siedler, G., M. Rouault, and J. R. E. Lutjeharms (2006), Structure and origin of the subtropical South Indian Ocean Countercurrent, *Geophysical Research Letters, 33*, L24609, doi:10.1029/2006GL027399.

Stramma, L., and J. R. E. Lutjeharms (1997), The flow field of the subtropical gyre of the South Indian Ocean, *Journal of Geophysical Research*, *102*, C3, 5513 – 5530.

Swallow, J, M. Fieux, and F. Schott (1988), The Boundary Currents East and North of Madagascar 1. Geostrophic Currents and Transports, *Journal of Geophysical Research,* 93, C5, 4951 – 4962.

van Leeuwen, P. J., Will P.M. de Ruijter, and J. R. E. Lutjeharms (2000), Natal pulses and the formation of Agulhas rings. *Journal of Geophysical Research, 105, C3, 6425 – 6436.*

Figure captions

1.

Schematic surface currents (thin solid arrows) in the southwestern Indian Ocean (MOZ_CH = Mozambique Channel, MOZ_B = Mozambique Basin, MAD_P = Madagascar Plateau, MAD_B = Madagascar Basin, WIL_R = Wilshaw Ridge, MAS_P = Mascarene Plateau). The shading indicates isobaths with 1000 m separation where greater depths correspond to darker shading. The thick open arrows give a simplified pattern of the subtropical gyre following Stramma and Lutjeharms (1997).

2.

Map of altimeter-derived surface geostrophic currents (06 November 2002, 5-day period) with color indicating speed and the arrows (only every second arrow plotted) presenting velocity.

3.

Geostrophic surface currents (only every second arrow plotted) derived from altimeter data averaged over (a) the second half of 2002, (b) the full year 2002, (c) the two years 2002 – 2003, and (d) the three years 2002 – 2004 (SEC = South Equatorial Current; SEMC = southern East Madagascar Current; SICC = South Indian Ocean Countercurrent).

4.

Sample of flow at 100 m from the model, with speed (color bar in m/s) and velocity (every 4th vector shown) as a 5-day average centered around 22 February 1993. Please note the

well-represented circulation pattern which is known from observations: the westward South Equatorial Current north of Madagascar, partially leading into southward flow through the Mozambique Channel between Madagascar and the African continent, the Agulhas Current along the South African coastline and the retroflection into the eastward Agulhas Return Current between 35 and 45° S. For a discussion of the flow east and south of Madagascar please see text.

5.

Sea surface height (SSH) maps averaged over 3 years from 01 January 2001 to 31 December 2003, with an isoline interval of 2.5 cm: (a) Aviso altimeter data, (b) model data. The thick lines indicate the 225 cm contour line in (a) and the 220.1 cm contour line in (b).

6.

One-month mean distributions for (a) July 2005 and (b) November 2005 showing the modes in SeaWiFS-derived chlorophyll_a patterns and corresponding altimeter-derived geostrophic surface current patterns. The positions of the chlorophyll_a sub-figures on the left are indicated in the surface current sub-figures on the right.

7.

Cyclonic (a) and anticyclonic (b) EKE for currents below the Ekman layer at 100 m from the model and cyclonic (c) and anticyclonic (d) EKE for surface currents from altimeter observations, averaged from 1 Jan 1996 to 31 Dec 2005. The boxes refer to Fig. 8. Units are $cm^2\ s^{-2}$. Please note the different scaling for the upper and lower sub-figures.

8.

Fractions of cyclonic (a) and anticyclonic (b) EKE from the model and fractions of cyclonic (c) and anticyclonic (d) EKE from altimeter observations relative to the mean EKE, averaged from 1 Jan 1996 to 31 Dec 2005. The boxes approximate regions of maximum fractions of EKE in the SEMC extension, with solid-line boxes referring to the particular sub-figure and broken-line boxes given for reference.

9.

Patterns of cyclonic (above) and anticyclonic (below) eddy tracks near Madagascar obtained from altimeter-derived SSH anomalies for eddy lifetimes longer than 16 weeks (courtesy of D. Chelton).

10.

Schematic representation describing the modes of the SEMC extension. The shading indicates isobaths with 1000 m separation where greater depths correspond to darker shading.

11.

Time series of altimeter vorticity magnitudes (absolute values) in the boxes given in Fig. 8: (a) 5-day altimeter data and (b) 2-month moving average of altimeter data.
Time series of model vorticity magnitudes in the boxes given in Fig. 8 and model transports at 21° S (green line): (c) 5-day model data and (d) 2-month moving average of model data.

12.

Cross-correlation sequence of SEMC transport at 21° S and cyclonic and anticyclonic motion in the boxes given in Fig. 8 from model data. The horizontal lines indicate the 95 % confidence level.

13.

Example float trajectories from the quantitative Lagrangian analysis. Particles were seeded along the double line at 21°S across the SEMC up to 1500m depth, advected by the model velocity and received and summed up at certain control sections (single lines). The control sections (clockwise labeled as NORTH, EAST, SOUTH, WEST and MOZ) are given in Tab. 2 (INI is the portion leaving the SEMC northward, DEPTH the portion below 1500m).

14.

As Fig. 13, but floats seeded at 55°E over the SICC and backwards calculated. The transports over the control sections are given in Tab. 3.

Table 1

Total Eddy Kinetic Energy (EKE) and fractions of cyclonic/anticyclonic EKE versus total EKE in the boxes defined in Fig. 8.

	Altimetry		**Model**	
Region	**cyclonic**	**anticyclonic**	**cyclonic**	**anticyclonic**
Box coordinates	40-43.5^{o}E 26.5-28.5^{o}S	40-43.5^{o}E 28.5-30.5^{o}S	43-44^{o}E 26-27^{o}S	43-44^{o}E 27.5-28.5^{o}S
Box area	76230 km^{2}	74738 km^{2}	11041 km^{2}	10890 km^{2}
Total EKE per unit area ($m^2s^{-2}m^{-2} = s^{-2}$)	2.2e-10	1.7e-10	1.4e-10	2.8e-10
Cyclonic EKE per unit area (s^{-2})	1.3e-10	8.4e-11	1.0e-10	9.8e-11
Fraction	0.59	0.51	0.70	0.35
Anticyclonic EKE per unit area (s^{-2})	8.9e-11	8.2e-11	4.4e-11	1.8e-10
Fraction	0.41	0.49	0.30	0.65

Table 2

Volume transports and corresponding percentages for the sections given in Fig. 13.

Section	Transport (Sv)	Percentage (%)
INI	3.82	24
DEPTH	0.03	0
NORTH	0.97	6
EAST	1.78	11
SOUTH	1.70	11
WEST	5.82	36
MOZ	1.90	12
TOTAL	**16.02**	**100**
CENTRAL INDIAN	6.60	41
AGULHAS	7.72	48

Table 3

Volume transports and corresponding percentages for the sections given in Fig. 14.

Section	Transport (Sv)	Percentage (%)
INI	4.15	48
DEPTH	0.05	1
NORTH	3.40	40
EAST	0.24	3
SOUTH	0.63	7
WEST	0.04	0
MOZ	0.06	1
TOTAL	**8.57**	**100**
CENTRAL INDIAN	7.84	91
AGULHAS	0.10	1

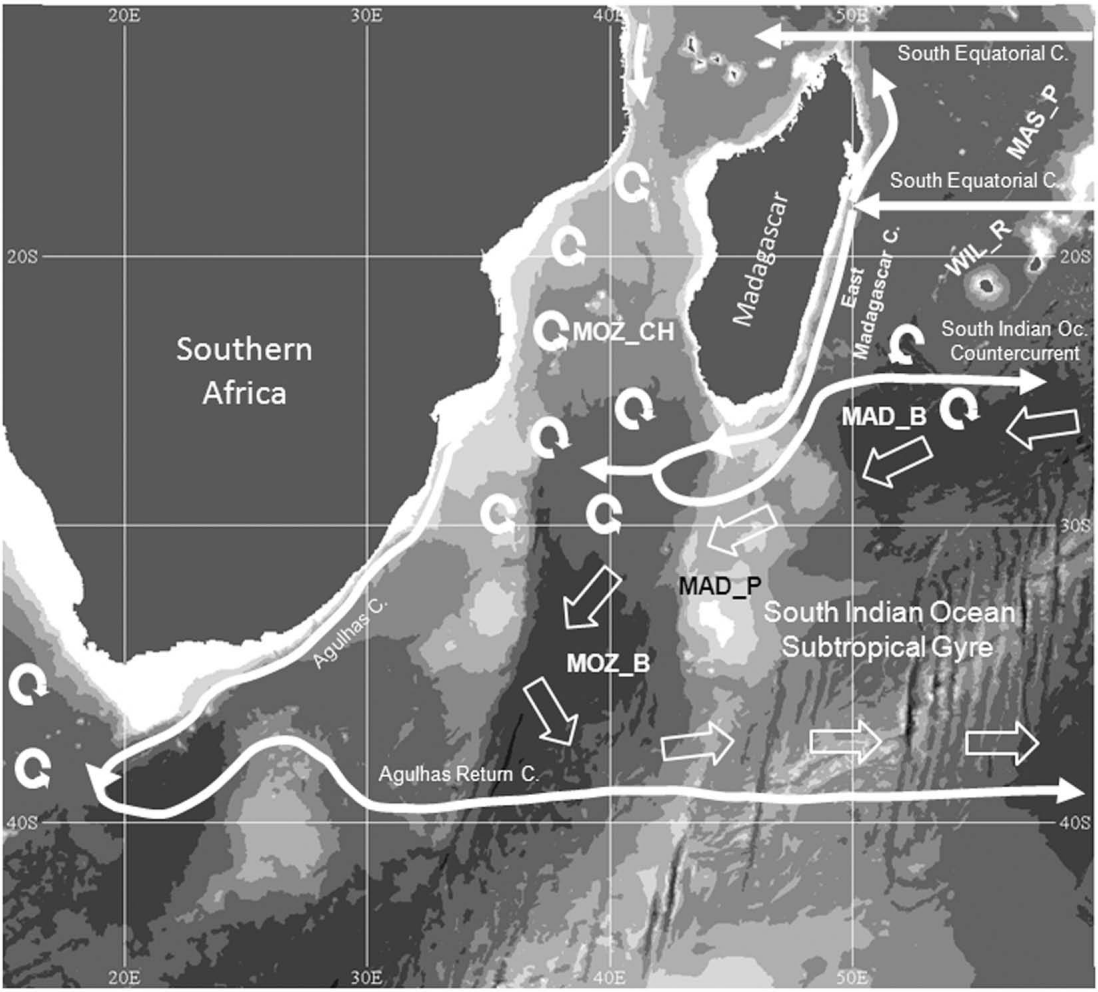
20E
30E
40E
50E
South Equatorial C.
MAS_P
South Equatorial C.
20S
Madagascar
East Madagascar C.
WIL_R
20S
Southern Africa
MOZ_CH
South Indian Oc. Countercurrent
MAD_B
30S
MAD_P
South Indian Ocean Subtropical Gyre
Agulhas C.
MOZ_B
Agulhas Return C.
40S
40S
20E
30E
40E
50E

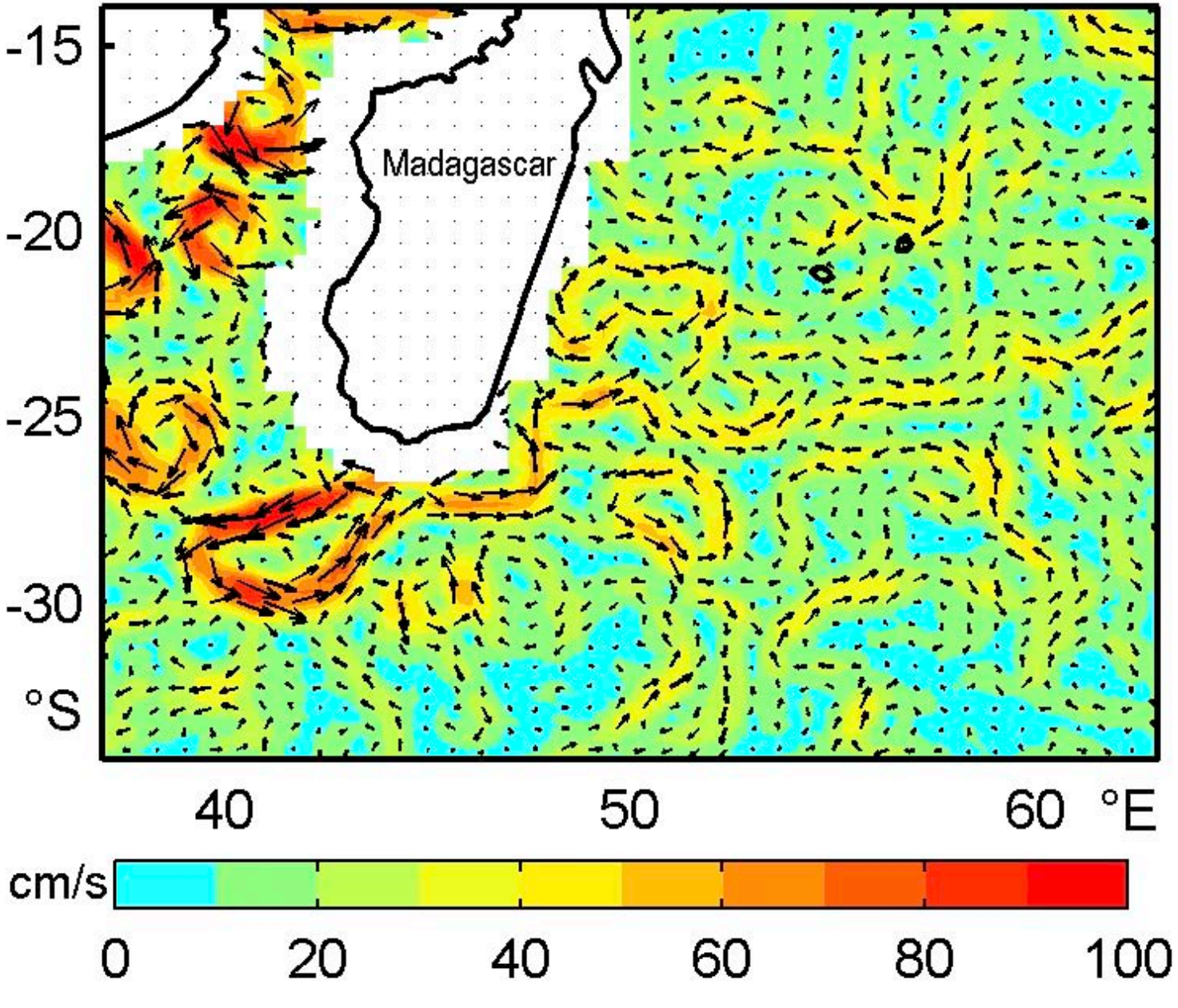
-15
-20
-25
-30
°S
Madagascar
40
50
60
°E
cm/s
0
20
40
60
80
100

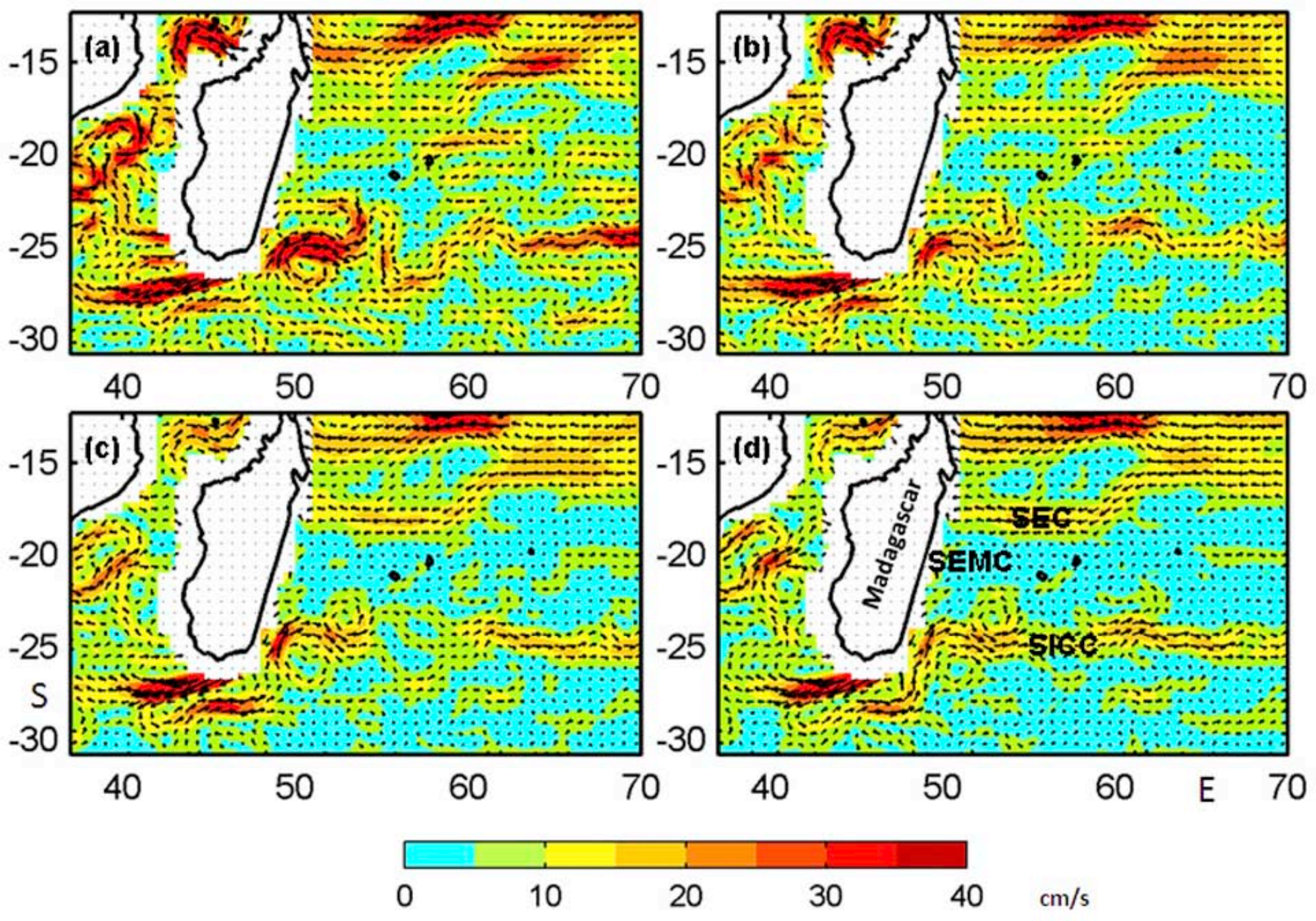
(a)
(b)
(c)
(d)
-15
-20
-25
-30
S
40
50
60
70
E
Madagascar
SEC
SEMC
SICC
0
10
20
30
40
cm/s

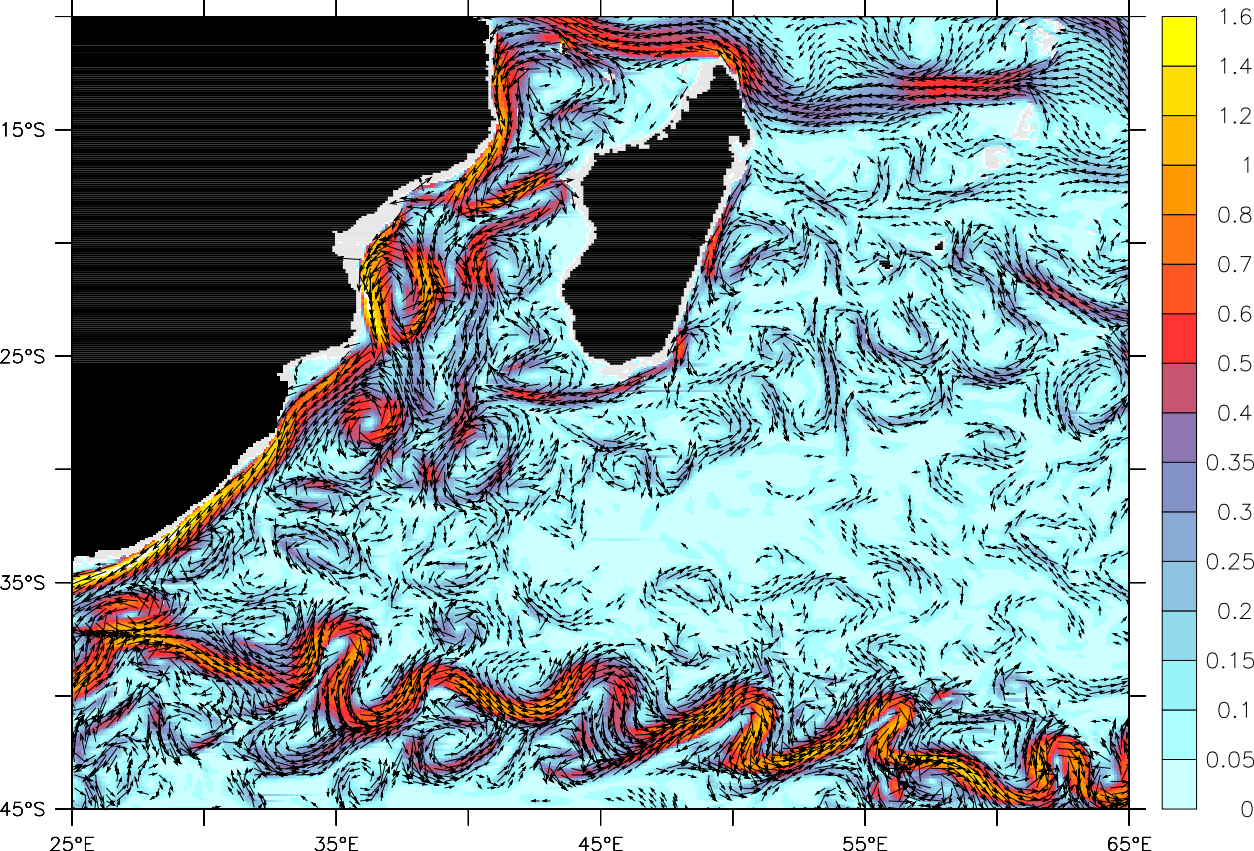
15°S
25°S
35°S
45°S
25°E
35°E
45°E
55°E
65°E
1.6
1.4
1.2
1
0.8
0.7
0.6
0.5
0.4
0.35
0.3
0.25
0.2
0.15
0.1
0.05
0

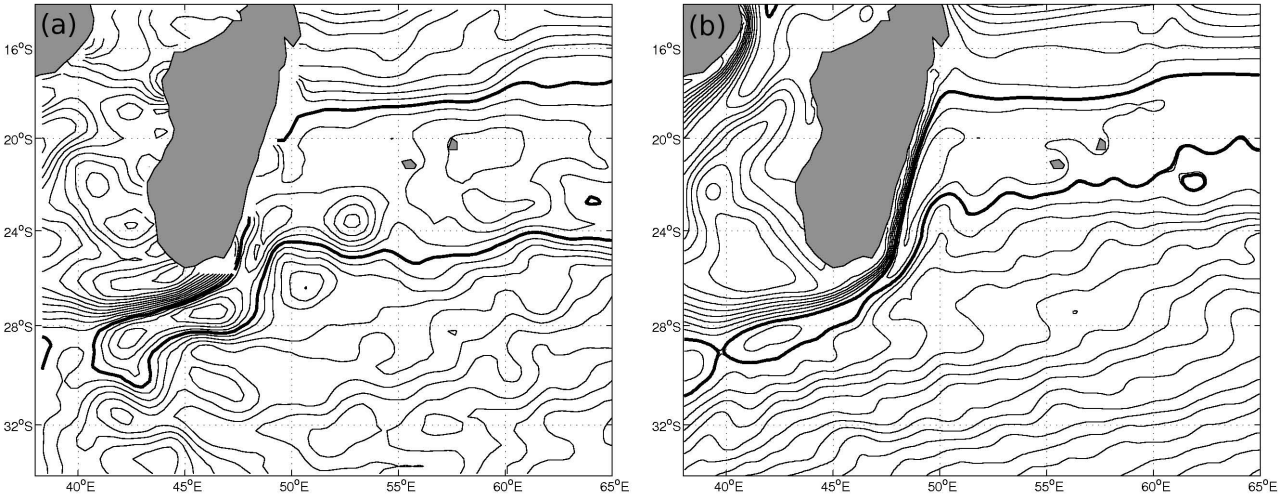
(a)
(b)
16°S
20°S
24°S
28°S
32°S
40°E
45°E
50°E
55°E
60°E
65°E

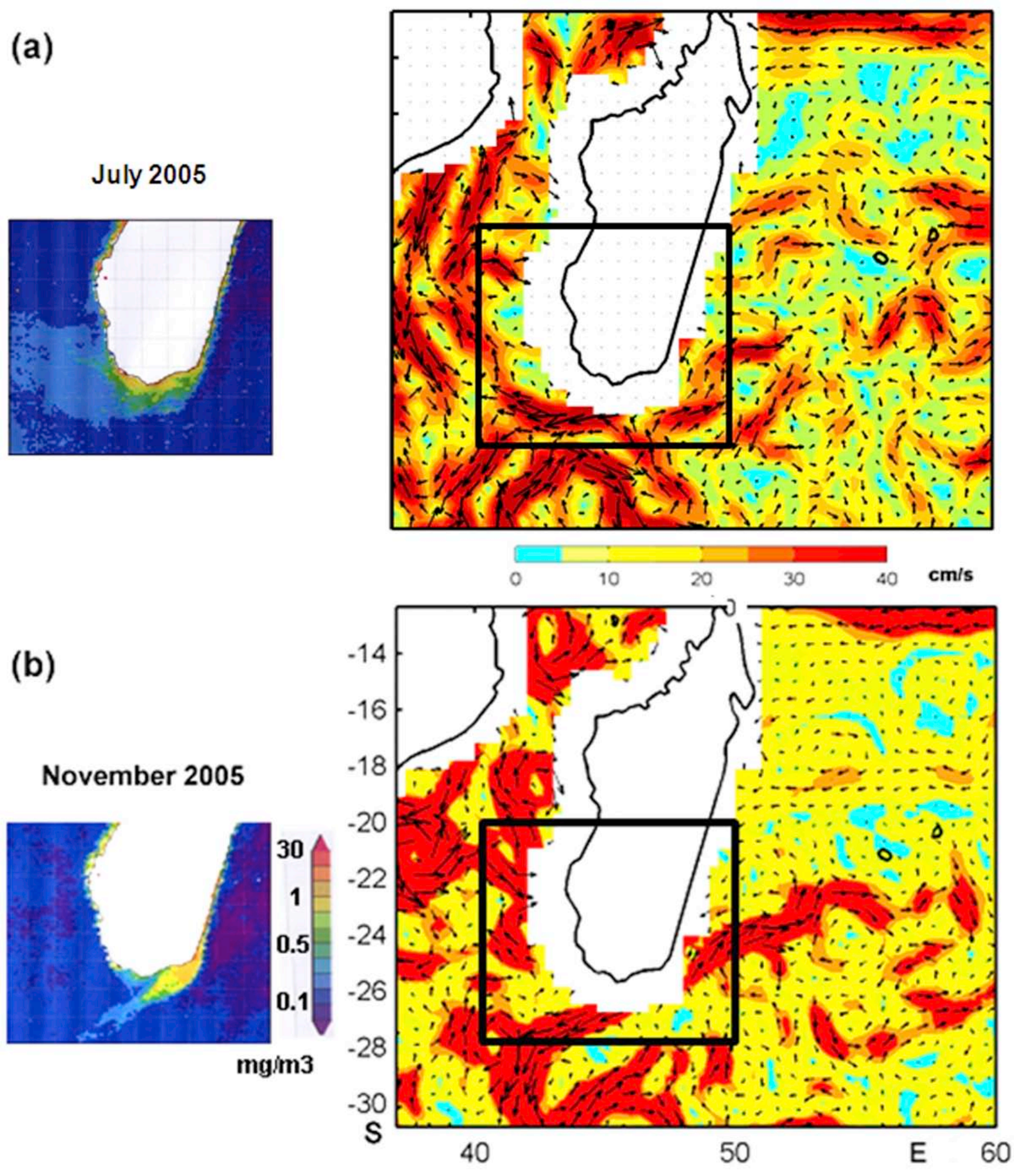
(a)
July 2005
0
10
20
30
40
cm/s
(b)
November 2005
30
1
0.5
0.1
mg/m3
-14
-16
-18
-20
-22
-24
-26
-28
-30
S
40
50
E
60

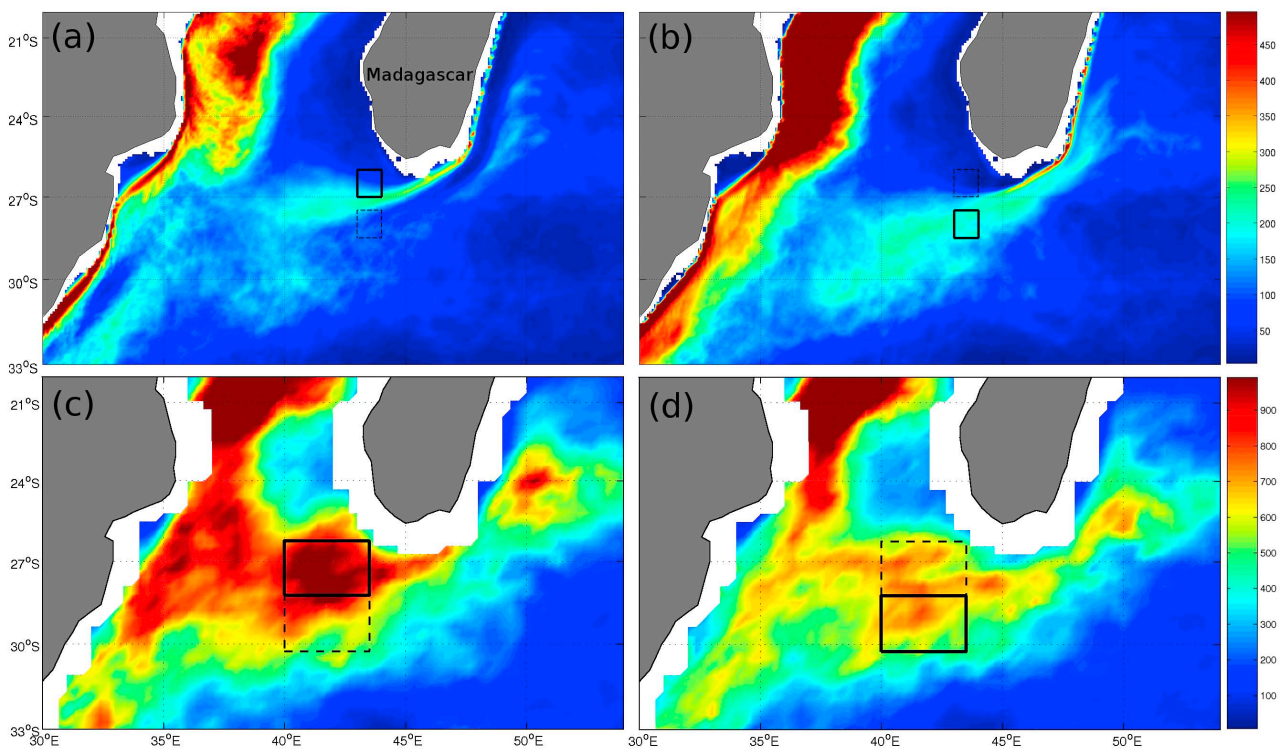
(a)
(b)
(c)
(d)
Madagascar
21°S
24°S
27°S
30°S
33°S
30°E
35°E
40°E
45°E
50°E
450
400
350
300
250
200
150
100
50
900
800
700
600
500
400
300
200
100

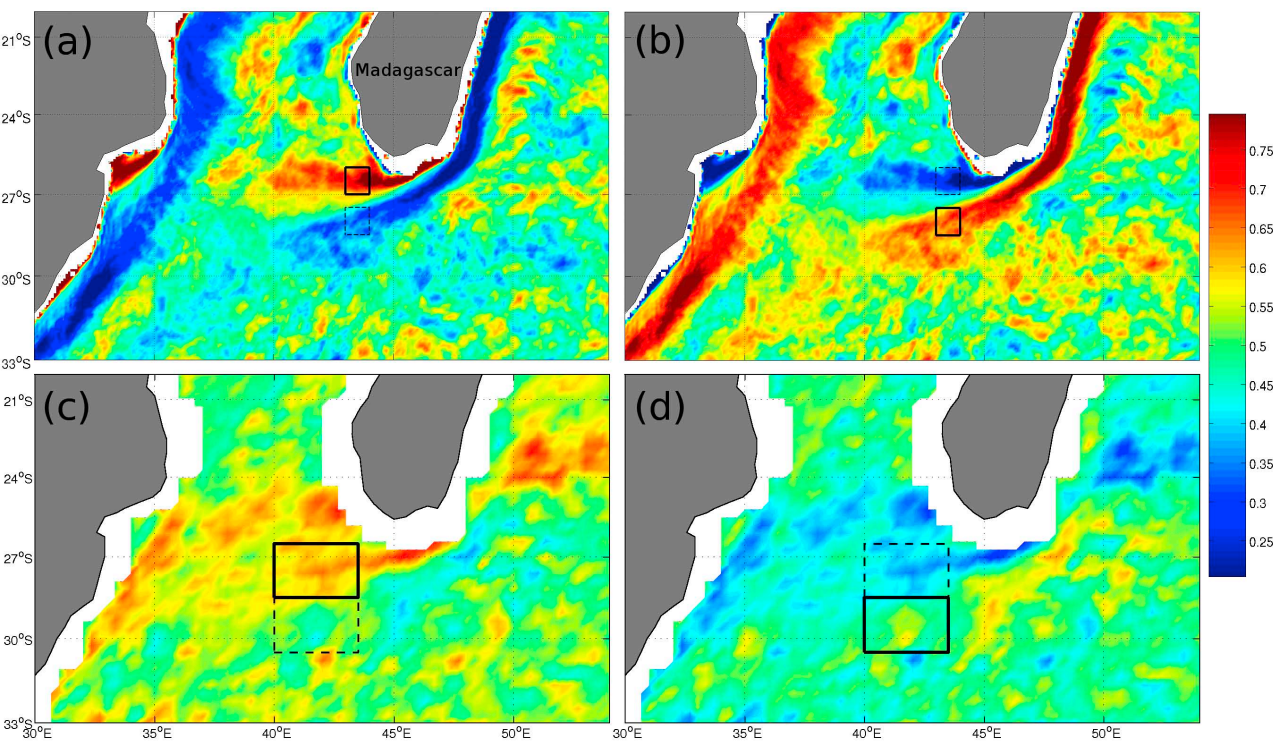
(a)
(b)
(c)
(d)
Madagascar
21°S
24°S
27°S
30°S
33°S
30°E
35°E
40°E
45°E
50°E
0.75
0.7
0.65
0.6
0.55
0.5
0.45
0.4
0.35
0.3
0.25

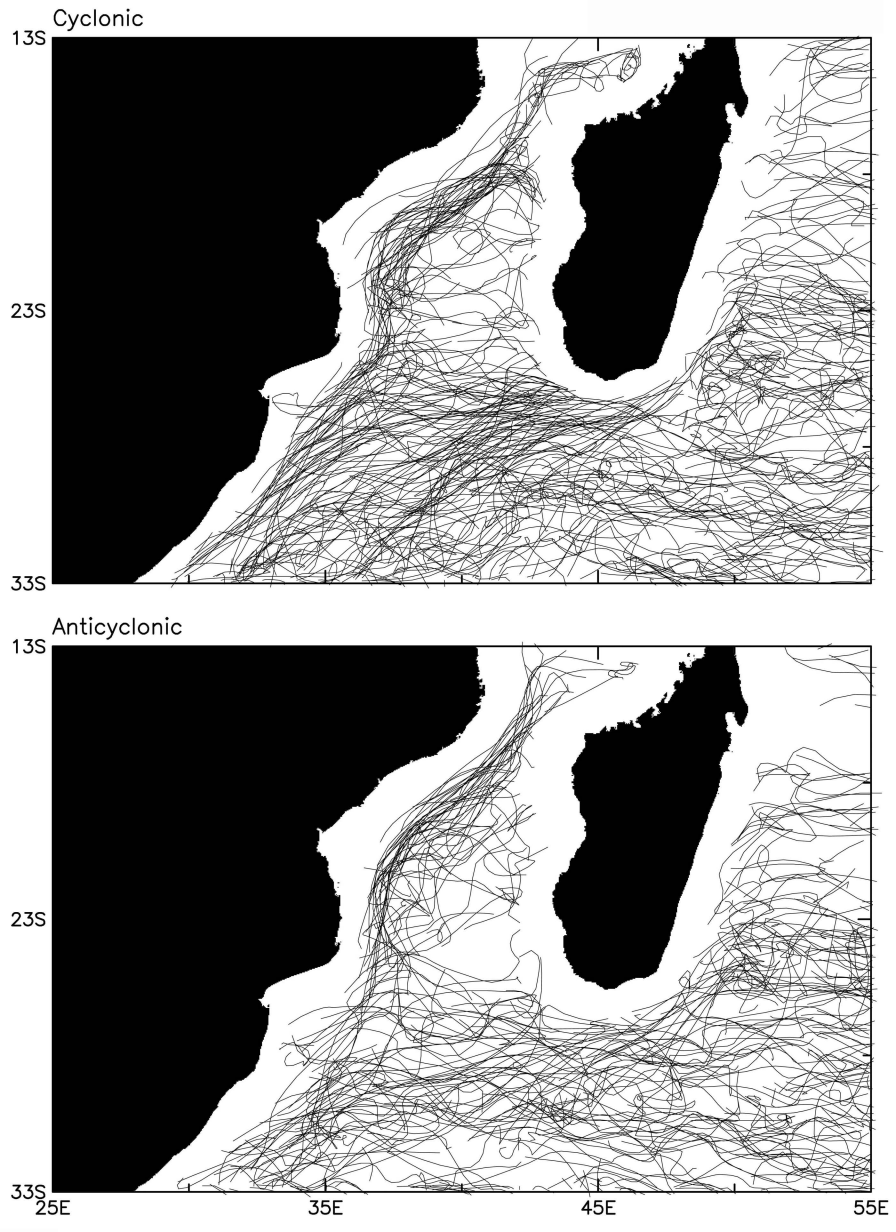
Cyclonic
13S
23S
33S
Anticyclonic
13S
23S
33S
25E
35E
45E
55E

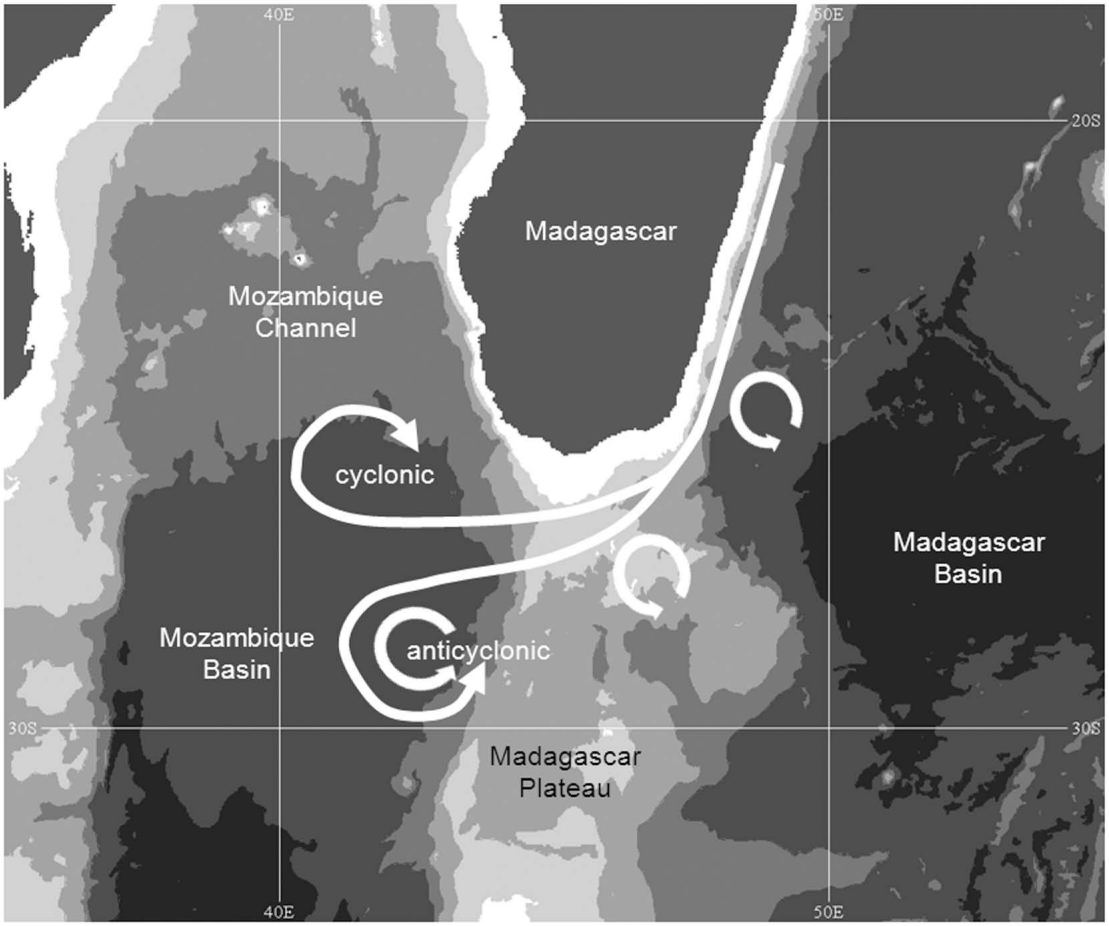
40E
50E
20S
30S
Madagascar
Mozambique
Channel
cyclonic
Madagascar
Basin
Mozambique
Basin
anticyclonic
Madagascar
Plateau

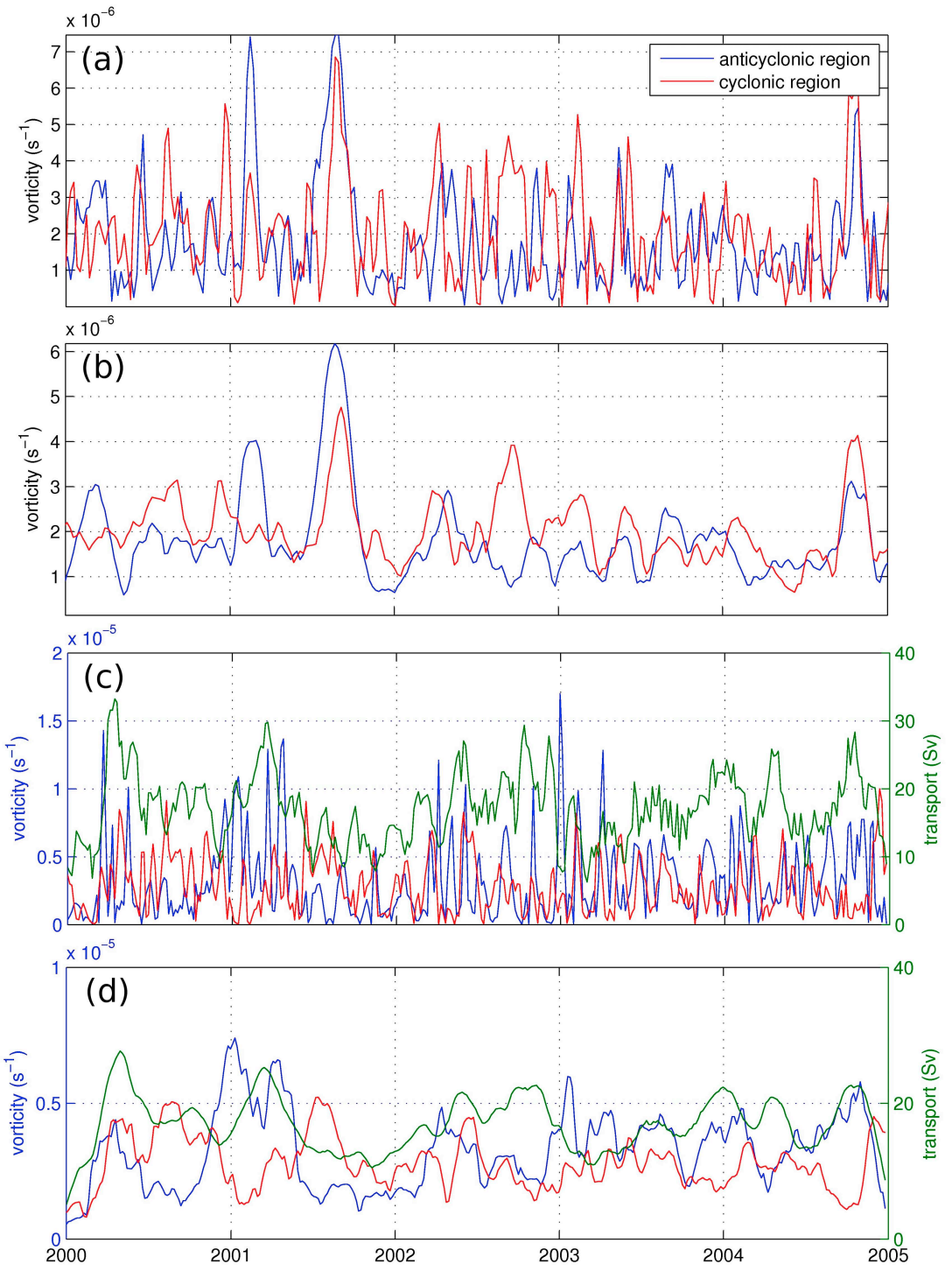
(a)
x 10^-6
vorticity (s^-1)
anticyclonic region
cyclonic region
(b)
x 10^-6
vorticity (s^-1)
(c)
x 10^-5
vorticity (s^-1)
transport (Sv)
(d)
x 10^-5
vorticity (s^-1)
transport (Sv)
2000
2001
2002
2003
2004
2005

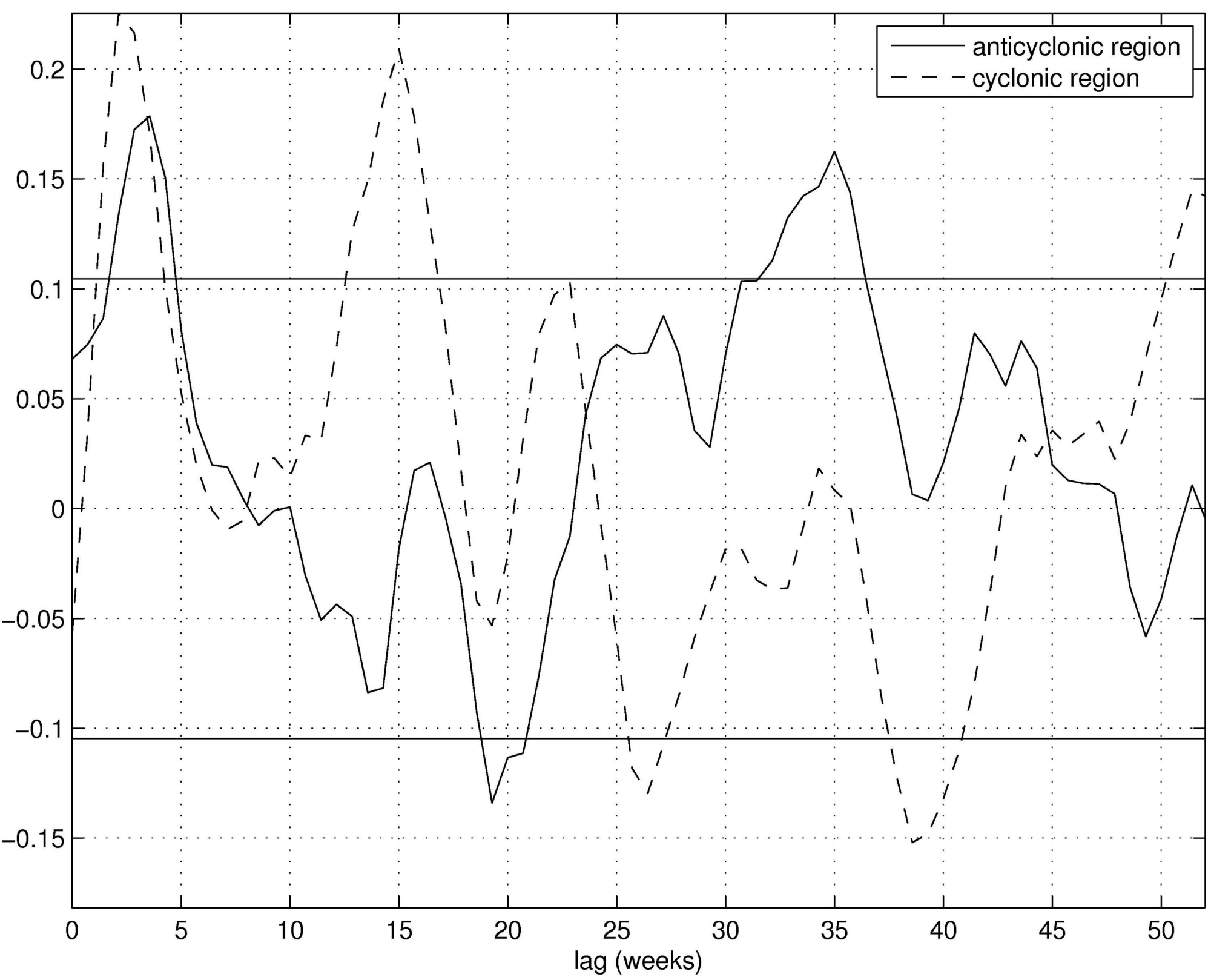
anticyclonic region
cyclonic region
0.2
0.15
0.1
0.05
0
−0.05
−0.1
−0.15
0
5
10
15
20
25
30
35
40
45
50
lag (weeks)

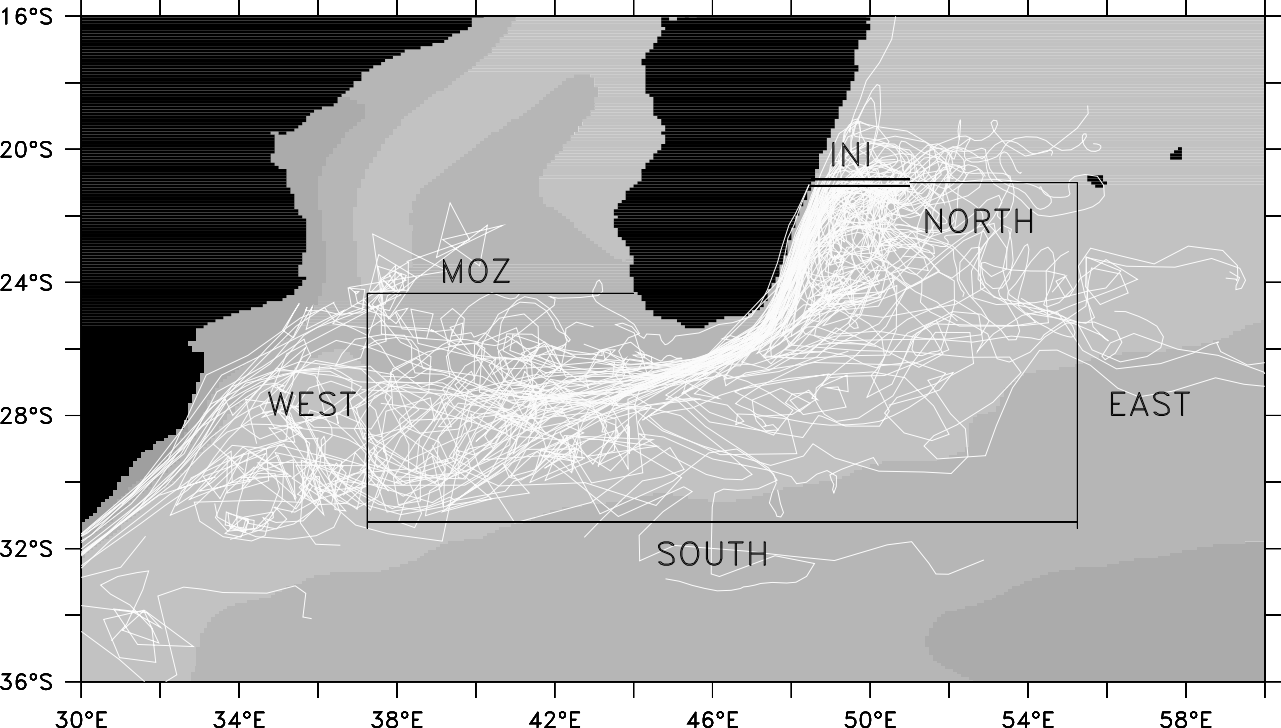
16°S
20°S
24°S
28°S
32°S
36°S
30°E
34°E
38°E
42°E
46°E
50°E
54°E
58°E
INI
NORTH
MOZ
WEST
EAST
SOUTH

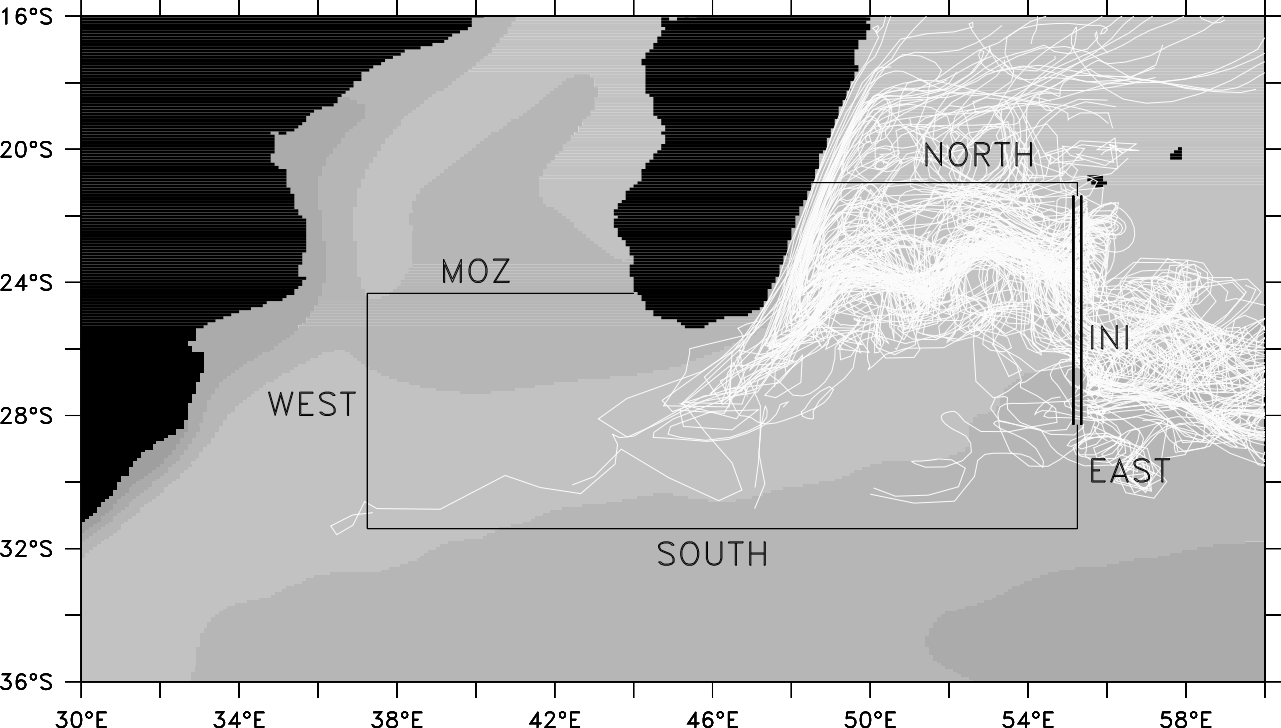
16°S
20°S
24°S
28°S
32°S
36°S
30°E
34°E
38°E
42°E
46°E
50°E
54°E
58°E
NORTH
MOZ
INI
WEST
EAST
SOUTH